Available online at www.sciencedirect.com
SCIENCE DIRECT
Tectonophysics 416 (2006) 209–228
TECTONOPHYSICS
www.elsevier.com/locate/tecto

Identification of crustal and upper mantle heterogeneity by modelling of controlled-source seismic data

L. Nielsen*, H. Thybo

Geological Institute, University of Copenhagen, Denmark

Accepted 28 November 2005
Available online 7 February 2006

Abstract

High-frequency controlled-source seismic sections with dense spatial sampling show the existence of heterogeneity at different depth levels of the continental crust and upper mantle. Our sources of information are the Peaceful Nuclear Explosion (PNE) seismic data sets recorded to large offsets in the former Soviet Union supplemented by recordings from the North American Early Rise deep seismic experiment and normal-incidence reflection seismic sections collected in northwest Europe.

Heterogeneity in the crust and upper mantle can be uniquely identified in reversed high-frequency (2–10 Hz) PNE seismic sections collected with dense spatial sampling (nominal receiver spacing of 10–15 km) out to 4000 km offset. We document pronounced seismic scattering from three heterogeneous zones: The lower crust from ~20 km to ~40 km depth, an ~80 km thick low-velocity zone below ~100 km depth, and the ~320–460 km depth interval around the top of the mantle transition zone. We calculate the full seismic wavefield in heterogeneous crust–mantle models with a two-dimensional finite-difference algorithm. We represent the heterogeneous layers by random fluctuations of the elastic parameters and Q-values. The spatial (horizontal and vertical) correlation lengths and the standard deviation of the scattering media are constrained by comparison of observed and calculated seismic sections.

The lower crustal heterogeneity causes a coda to the upper mantle arrivals at all recorded frequencies. This coda is a prominent feature for whispering-gallery phases (teleseismic Pn), which travel as multiply reflected refractions below the Moho to more than 3000 km offset from the PNE sources.

The heterogeneous mantle low-velocity zone causes a scattered coda trailing the first arrivals in the ~800–1400 km offset range. The best fit to the observations along profile Kraton in Siberia is obtained by an 80 km thick heterogeneous low-velocity zone below 100 km depth, represented by fluctuations described by a von Karman distribution function with a Hurst number of 0.5 and spatial correlation lengths of 5–10 km (horizontally) and 3–5 km (vertically).

Scattered arrivals, which trail the reflection from the '410' discontinuity and a reflection from a shallower depth of ~320 km, constrain heterogeneity around the top of the transition zone. This heterogeneity is modelled by fluctuations in the 320–460 km depth interval with correlation lengths on the order of 20–40 km by 5–10 km. Scattering from the two shallower heterogeneous zones improves the description of the phases from around the transition zone.

Keywords: Mantle; Crust; Seismic scattering; Seismic modelling; Peaceful nuclear explosions

* Corresponding author.
E-mail address: ln@geol.ku.dk (L. Nielsen).

0040-1951/$ - see front matter © 2005 Elsevier B.V. All rights reserved.
doi:10.1016/j.tecto.2005.11.020

1. Introduction

Detailed description of heterogeneity in the Earth's crust and mantle is necessary for identification of chemical and phase changes, mapping of anisotropic layers, and description of thermal and rheological variations. These factors are important for our understanding of the creation of the crust–mantle system and plate tectonic processes.

Seismic methods constitute the strongest tools for detailed mapping of small-scale heterogeneity in large volumes of the Earth. During the last 20–30 years, tomographic inversion of seismic signals recorded from earthquakes on global networks has provided new two- and three-dimensional images of the deep Earth (e.g., Ekström and Dziewonski, 1998; Bijwaard and Spakman, 2000). The tomographic methods have provided new information about the overall seismic velocity structure of the Earth's mantle with a resolution down to the order of 100 km by 100 km. The images have been interpreted to show mantle plumes, continental lithospheric roots and subducted slabs that penetrate the mantle to the transition zone at ~410 km depth and possibly to the core–mantle boundary (e.g. Fukao et al., 2001; Romanowicz and Gung, 2002; Montelli et al., 2004).

However, higher-resolution seismic data and methods can resolve mantle heterogeneity on a finer scale than tomographic inversion of global-network seismic data. Seismic waves recorded from powerful controlled sources, e.g. Peaceful Nuclear Explosions (PNEs) detonated in the former Soviet Union during the 1960s–1980s (Fig. 1), contain significantly higher frequencies than the signals recorded from earthquakes. Further, the seismic signals from the PNEs have been recorded with a dense spacing of 10–15 km between the receivers along 3000–4000 km long profile lines. Normally, three or four PNEs were distributed evenly along each line to provide reverse coverage of mantle arrivals (Fig. 1). The seismic signals generated by the PNEs have the potential to identify heterogeneity at km-scale in the Earth's crystalline crust and mantle down to the core–mantle boundary (e.g., Tittgemeyer et al., 1996; Thybo and Perchuc, 1997; Ryberg et al., 2000; Nielsen et al., 2002, 2003a; Thybo et al., 2003a,b; Ross et al., 2004). Seismic signals recorded from the large dynamite explosions of the Early Rise experiment in North America during the 1960s (Fig. 1) resolve mantle structures at about the same resolution as the PNEs, at least to the top of the mantle transition zone, although this data set is not reversed. High-frequency normal incidence data sections collected in e.g. northwest Europe (Fig. 1) resolve crustal and uppermost mantle layering on a vertical scale of ~100 m to depths of 80–100 km. Further, the availability of controlled-source seismic data from different continental regions provides strong bounds on heterogeneity characteristics, which are probably general features of the continental crust and mantle.

Here, we review controlled-source seismic observations and modelling results, which document the

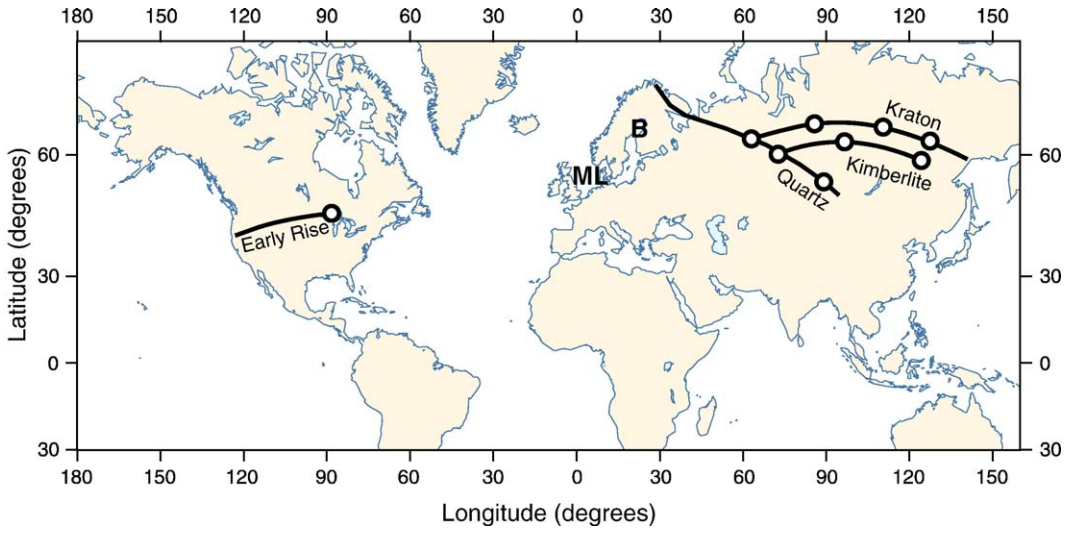

Fig. 1. Seismic data locations. Bold lines mark locations of receivers that recorded the seismic waves from powerful sources (circles). Sources located in the former Soviet Union are so-called "Peaceful Nuclear Explosions" (PNEs). The Early Rise source detonated in Lake Superior in North America consisted of 30 tonnes of explosives. B and ML mark the positions of the normal-incidence reflection seismic surveys BABEL and MONA LISA, respectively (cf. BABEL Working Group, 1993; MONA LISA Working Group, 1997).

existence of heterogeneity in three well-defined depth intervals of the continental crust and upper mantle: 1) the lower crust from about 20 to 40 km depth; 2) a 50–100 km thick low-velocity zone below ~100 km depth in cratonic areas; and 3) the ~320–460 km depth interval around the top of the mantle transition zone. We model the heterogeneity of these three heterogeneous zones by fluctuations described by von Karman correlation functions with Hurst numbers between 0.3 and 0.5. These correlation functions are characterised by specific spatial correlation lengths, but the functions include fluctuations over a broad wavenumber interval (e.g. Tittgemeyer et al., 1999; Nielsen et al., 2002). For Hurst numbers lower than 0.3, the von Karman functions exhibit almost fractal behaviour (Holliger and Levander, 1992). Based on the evidence for crustal and upper mantle heterogeneity, we construct a composite model, which includes heterogeneous zones at all three depth intervals. By new numerical calculations, we show that synthetic seismograms calculated for this model match the observed long-range data in the entire offset interval from 0 to 2500 km.

Our seismic models of the crust and upper mantle allow us to identify crustal and upper mantle heterogeneity at km-scale.

2. Waveform modelling

Our investigations are based on calculation of synthetic seismograms for heterogeneous models with a two-dimensional visco-elastic finite-difference algorithm, which is based on the method described by Robertsson et al. (1994). The validity of the heterogeneous models is assessed by comparison of the calculated and observed seismic sections. Numerical methods are needed for such studies, because no analytical solution exists for the propagation of seismic waves in strongly heterogeneous media.

Different heterogeneous zones of the crust–mantle system each have their specific effect on the seismic wavefield. Lower crustal heterogeneity gives rise to seismic scattering phenomena, which are identified over a broad frequency range of 0–10 Hz. The scattered signals observed from the 100–180 km depth interval and the heterogeneous zone around the top of the transition zone are mainly observed in the 1–4 Hz frequency range, probably because of strong attenuation of the high-frequency part of the waves that travel in the low-velocity zone below 100 km depth. Scattering attenuation of the high frequencies in the lower crust may also explain the lower frequency content of the scattered arrivals from the low-velocity zone and the top of the transition zone.

We define the seismic models on regular grids of cells for the finite-difference calculations. The grid cell size and the time step size of the calculations are chosen based on stability criteria, which depend on the velocity distribution and the maximum frequency of the signals that are propagated through the model (cf. Robertsson et al., 1994). We ensure that the minimum wavelength propagated on the grid is sampled by at least five grid points. This requires a relatively small grid spacing of 75 m and time steps of only 3.09 ms in order to maintain stability of the finite-difference algorithm up to the maximum frequency of 10 Hz which is required in order to investigate the scattering phenomena caused by the heterogeneous lower crust. This results in a finite-difference grid with more than 85 million grid points for 2000 km long and 240 km deep models. A total of 97,000 time steps must be calculated in order to obtain 300 s long records. The synthetic seismograms used to study the scattering characteristics from the 100–180 km and 320–460 km depth intervals have been calculated using a source with a centre frequency of 2 Hz and a maximum frequency of 5 Hz. Here, a grid size of 170 m and time steps of 6 ms ensure numerical stability. This results in ~55 million grid points for 2500 km long and 500 km deep models, and 55,000 time steps are calculated in order to obtain 328 s long records. A 30 km wide damping zone with small Q-values is padded along the sides and bottom of the model. Test simulations have shown that this damping zone ensures that undesired edge effects (such as reflections from the model boundaries) are effectively suppressed.

The finite-difference waveform calculations are performed on multiprocessor supercomputers with large amounts of shared memory. One synthetic wavefield simulation in the finely gridded model for simulating the lower crustal scattering takes about 10 days on an SGI Origin 2000 if 8 processors are used for parallel computations. The calculations of scattering in the 100–180 and 320–460 km depth intervals, which only involves frequencies up to 5 Hz, are less demanding and require only 3–5 days with the same number of processors on the SGI Origin 2000. The same calculations are performed about 4 times faster on more modern supercomputers, such as the IBM pSeries 690 (Regatta).

3. Influence of crustal heterogeneity

The Russian PNE data only sparsely shows seismic refractions and primary reflections from

intra-crustal layers because the 10–15 km receiver spacing is too coarse to properly sample such phases. Nevertheless, interference of scattered arrivals caused by crustal heterogeneity gives rise to scattered wave trains (coda), which trail observed mantle arrivals.

Long-range P-wave arrivals, the so-called teleseismic Pn waves, are observed with an apparent upper mantle velocity of ~8.1–8.4 km/s to offsets of more than 3000 km along the PNE seismic profile Quartz (Fig. 2). The teleseismic Pn waves are characterized by a long (possibly up to more than 100 s) high-amplitude coda

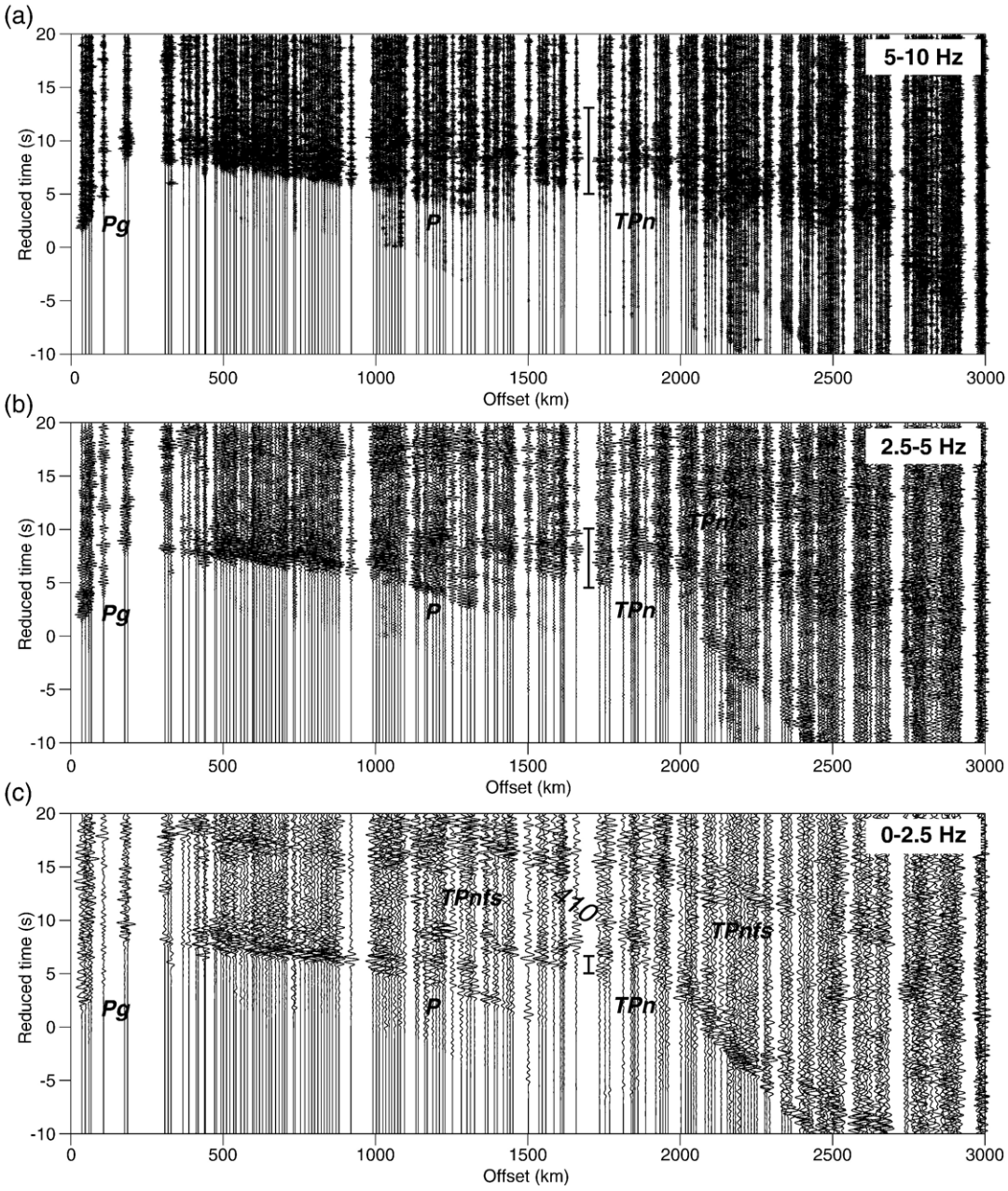

Fig. 2. Seismic data recorded from the southernmost shot point of PNE profile Quartz (cf. Fig. 1). The data are plotted in reduced travel time format (reduction velocity 8.0 km/s). Three different frequency ranges are plotted: 5–10 Hz (a), 2.5–5 Hz (b), and 0–2.5 Hz (c). Pg: Refracted wave in the crust. P: Refracted wave in the upper mantle. TPn: Teleseismic Pn wave. TPnfs: Free-surface multiple of the TPn and P–S converted waves. 410: reflection from the top of the mantle transition zone. Vertical bars indicate the approximate length of the directly observable coda of the TPn.

which is visibly observable in the record sections over ca. 8–10 s long time windows (cf. Ryberg et al., 1995; Tittgemeyer et al., 1996; Morozov and Smithson, 2000; Nielsen and Thybo, 2003).

The teleseismic Pn is evident at offsets larger than ~1000 km, where it detaches from the first arrival P-wave (Fig. 2). The travel time curve of the first arrival P-wave has significant curvature, indicating a high, positive vertical upper mantle velocity gradient. The first arrival is strongly attenuated at about 1500 km offset, probably due to an attenuating low-velocity zone in the ~120–135 km depth range below profile Quartz (cf., Ryberg et al., 1996; Morozova et al., 1999). This confirms the finding that the upper mantle low-velocity zone attenuates seismic waves (Thybo and Perchuc, 1997; Abramovitz et al., 2002; Nielsen et al., 2002; Selby and Woodhouse, 2002; Thybo, 2006).

The teleseismic Pn waves and their coda are observed over a broad frequency range from 0 to 10 Hz, and the amplitudes of the coda wave trains relative to the amplitude of the first wiggles of the teleseismic Pn are frequency dependent (Fig. 2). In the frequency interval from 0 to 2.5 Hz the teleseismic Pn appears with a sharp onset in part of the record section, and the amplitudes of the coda wave trains are weak compared to the onset amplitudes. In the mid-frequency range (2.5–5 Hz), the amplitudes of the first ~5–6 s of the coda wave train are similar to the amplitudes observed at the onset of the teleseismic Pn. For the high-frequency signals (5–10 Hz), the time interval over which the coda amplitudes are similar to the amplitudes of the onset of the teleseismic Pn is up to ~8–10 s long. There is also a coda to the first arrival P-wave in the ~200–1500 km offset range with similar frequency characteristics as the teleseismic Pn arrival. In general, the coda to the first arrivals appears to be 2–3 s shorter than the coda of the teleseismic Pn.

We have tested two fundamentally different models of generation of the teleseismic Pn arrival and its coda. The first model includes a 20 km thick heterogeneous lower crust, and the upper mantle does not contain heterogeneity to 100 km depth (Model 1; Fig. 3a) (Nielsen and Thybo, 2003). The uppermost mantle has a strong, positive vertical velocity gradient, which is a characteristic of the Russian cratonic regions (Ryberg et al., 1996; Morozova et al., 1999; Nielsen et al., 1999). The lower crustal heterogeneity is described by a von Karman distribution function with a Hurst number of 0.3 and horizontal and vertical correlations lengths of 2.4 and 0.6 km, respectively. Media described by a von Karman distribution function are relatively rough, because a broad range of wavenumber contribute to the heterogeneity spectrum. The Hurst number, which can take on a value between 0 and 1, controls the correlation decay. Small Hurst numbers result in a more rapid decay than large numbers. The second model (Ryberg et al., 2000) is described by a homogeneous crust and a heterogeneous mantle from 40 to 100 km depth (Model 2; Fig. 3b). The horizontally elongated upper mantle fluctuations follow a Gaussian distribution function with correlation lengths of 20 km (horizontally) and 0.5 km (vertically). Such smooth fluctuations ensure that the upper mantle appears non-reflective at high frequencies, as observed in normal-incidence seismic sections. However, all observed heterogeneity in nature typically requires a fractal-like description, which is not the case for at Gaussian distribution function.

The calculated visco-elastic seismic responses of the two test models are compared to the observed data sections (Fig. 4). In Model 1 the teleseismic Pn wave propagates to far offsets as multiply reflected refractions along the underside of the Moho due to the positive vertical upper mantle velocity gradient (Fig. 3c). This model provides a good fit to the observed data. It successfully reproduces the key observations in all three frequency ranges: the curvature of the first arrival P-wave; the apparent velocities of 8.1–8.4 km/s of the teleseismic Pn wave; the detachment of the teleseismic Pn arrival from the first arrival P-wave at ~1000 km offset; the visual duration of the teleseismic Pn coda; and the termination of the Pn arrival at ~1600 km offset. In Model 2 the upper mantle acts as a scattering waveguide to the seismic wavefield (Ryberg et al., 2000) (Fig. 3d). This model only explains the observed high-frequency characteristics of the teleseismic Pn coda. In the low-frequency (0–2.5 Hz) and mid-frequency (2.5–5 Hz) ranges, the upper mantle scattering waveguide produces a far too extensive coda with relatively large amplitudes. Moreover, Model 2 cannot explain the observed kinematic differences between the first arrival P-wave and the teleseismic Pn, i.e. the model does not properly reproduce the detachment of the teleseismic Pn from the first arrival P-wave at ~1000 km offset, nor does it explain the first-arrival phase out to ~1600 km offset.

Nielsen and Thybo (2003) discuss the seismic responses of the two principal models in more detail and show results from a series of wavefield simulations. They conclude that the upper mantle scattering models cannot fit the kinematics of the direct P-wave and the teleseismic Pn, regardless of the choice of the vertical velocity gradient. In contrast, Model 1, which includes lower crustal heterogeneity and a transparent uppermost mantle with a large positive vertical velocity gradient to

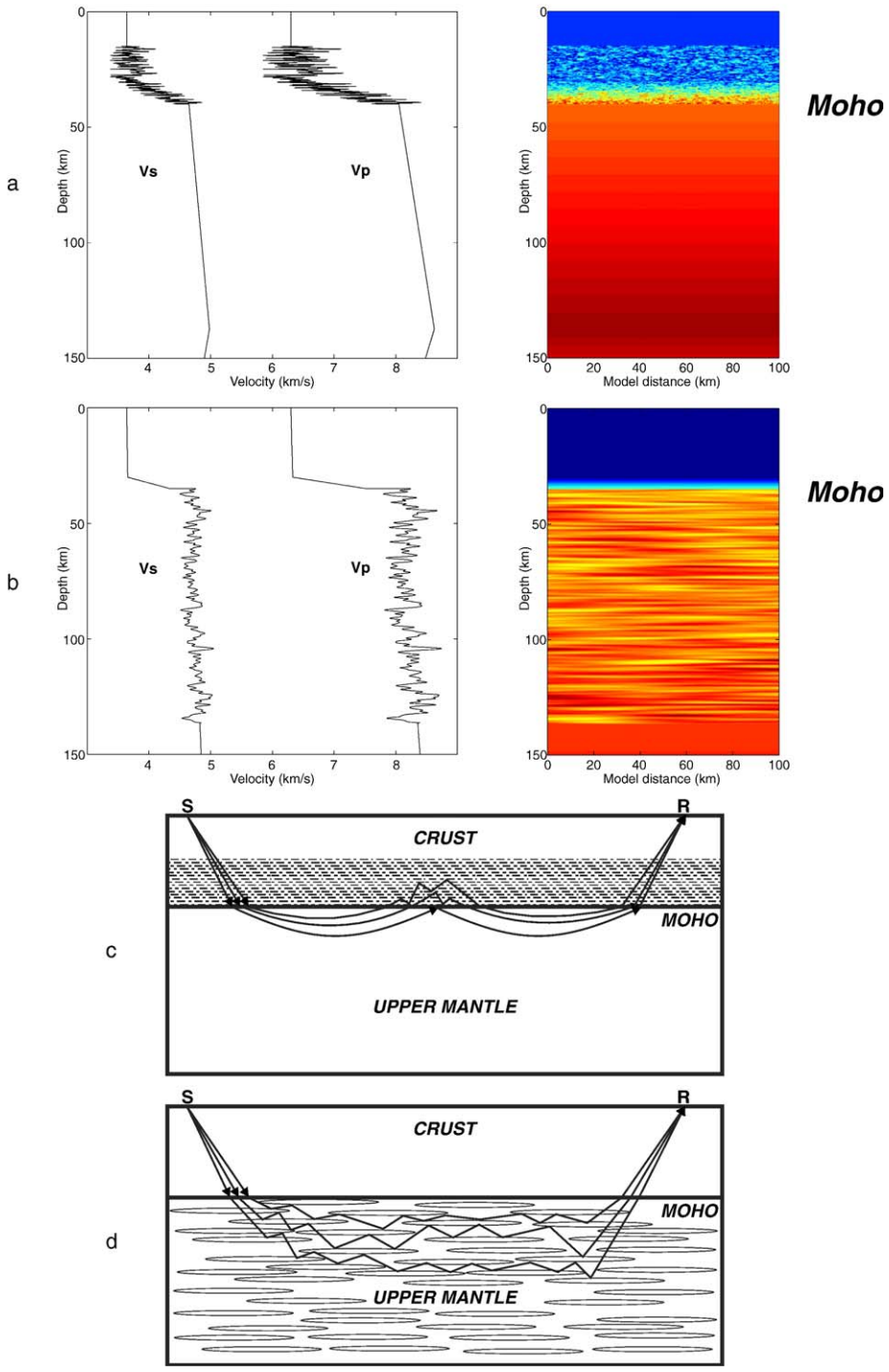

Fig. 3. Preferred (a) and rejected (b) velocity models for explaining the teleseismic Pn phase. In (a) and (b), 1D Vp and Vs velocity profiles (left) are extracted from the 2D velocity models (right) at 3.4 km model distance. Only 100 km of the 2000 km long 2D models are shown. In (a) the lower crustal velocity fluctuations from 15 to 40 km depth follow a von Karman distribution function with a Hurst number of 0.3 and horizontal and vertical correlation lengths of 2.4 km and 0.6 km, respectively (Nielsen and Thybo, 2003). In (b) the crust is transparent and the fluctuations of the upper mantle follow a Gaussian distribution function with horizontal and vertical correlation lengths of 20 km and 0.5 km, respectively (Ryberg et al., 2000). Sphericity of the earth is accounted for by applying the corrections of Müller (1985) to the velocity models. Schematic representations of ray paths of seismic waves propagating through the preferred model (c) and the rejected model (d).

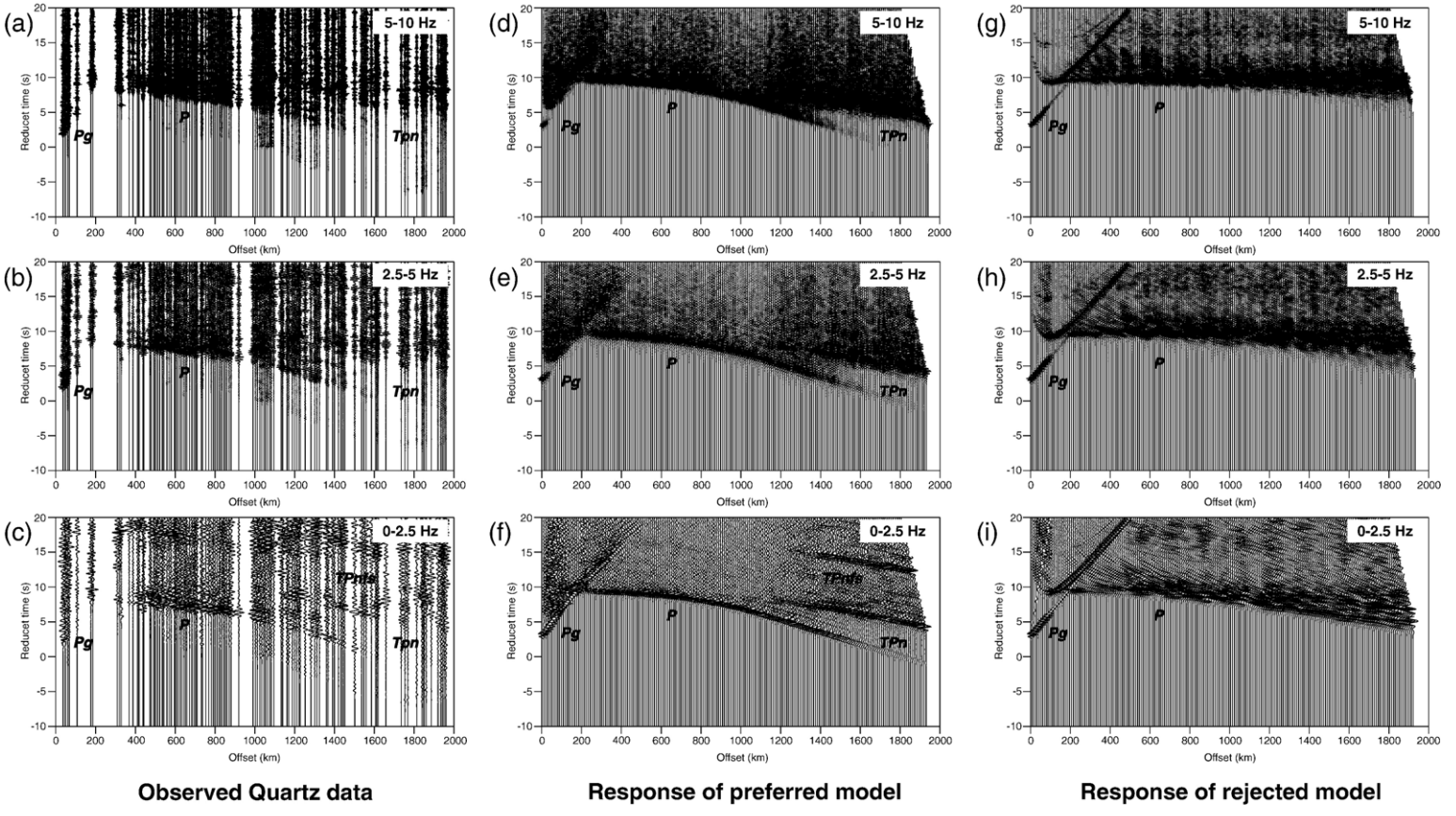

Fig. 4. Observed and calculated trace-normalized seismic data sections plotted in reduced travel time format (reduction velocity of 8.0 km/s) from 0 to 2000 km offset. Three different frequency ranges of the observed data from PNE profile Quartz are plotted: 5–10 Hz (a), 2.5–5 Hz (b), and 0–2.5 Hz (c). The same frequency ranges of the seismic data calculated for the preferred model (Fig. 3a) are plotted in (d)–(f). The background velocity model is a 1D average of the velocities found along profile Quartz (cf. Ryberg et al., 1996; Morozova et al., 1999). The three different frequency ranges of the seismic data calculated for the rejected model (Fig. 3b) are shown in (g)–(i). Pg: Refracted wave in the crust. P: Refracted wave in the upper mantle. TPn: Teleseismic Pn wave. TPnfs: Free-surface multiple of the TPn and P–S converted waves.

100 km depth, appears to be robust. Nielsen and Thybo (2003) demonstrate that a range of correlation lengths (0.8–2.6 km horizontally and 0.2–0.8 km vertically) of the lower crustal fluctuations explain the observed coda characteristics equally well. A positive upper mantle velocity gradient is required in order to propagate the teleseismic Pn as multiply reflected refractions along the underside of Moho. A large positive gradient will lead to a strong curvature of the travel time curves of the first arrival P-wave and teleseismic Pn arrivals as well as a clear detachment of the teleseismic Pn phase from the first arrival P-wave, whereas a small positive gradient will only result in a weak curvature of the travel time curves and small travel time differences between the teleseismic Pn and the first arrival P-wave (Nielsen et al., 2003b). A relatively large uppermost mantle velocity gradient of 0.0059 km/s/km provides a match between the kinematics of the teleseismic Pn and the first arrival P-waves along profile Quartz. Analysis of travel time data along the PNE seismic profiles located on the Russian craton has shown that a large positive upper mantle velocity gradient is a characteristic of the upper 40–50 km of the mantle in this area (Ryberg et al., 1996; Morozova et al., 1999; Nielsen et al., 1999). Based on our findings, we conclude that the kinematics of the teleseismic Pn phase can be explained by whispering-gallery phases that propagate along the underside of the Moho as multiply reflected refractions. We further conclude that the coda characteristics of the teleseismic Pn can be fully accounted for by crustal scattering, whereas the previously suggested model by Ryberg et al. (2000) (Model 2) cannot explain the teleseismic Pn coda by multiple upper mantle scattering and is in conflict with the observed data of PNE profile Quartz.

Similar coda characteristics of the teleseismic Pn have also been observed along PNE profile Ruby, which is sub-parallel to profile Quartz (Tittgemeyer et al., 1996). So far, these coda characteristics have not been documented along other seismic profiles and, therefore, they may be unique for the central and western Russian regions. We may speculate that the teleseismic Pn wave is only observed in the East European Platform area because of the requirement for an exceptionally large vertical velocity gradient. We are not aware of other regions with similar large vertical velocity gradients in the uppermost mantle or of other regions where a similar teleseismic Pn phase has been observed.

4. Heterogeneity in the 100–200 km depth interval

Scattered and delayed signals, which are consistently observed in the PNE seismic sections, give evidence for a 50–100 km thick heterogeneous low-velocity zone below ~100 km depth (Fig. 5). The delayed and scattered arrivals are present in the main frequency band of the PNE seismic sections (~2–4 Hz) with the following key characteristics: 1) the delays are up to ~2 s, and they always occur at offsets of 800–1000 km; 2) the scattered wave trains form a coda to the first arrivals at offsets larger than ~500–800 km (mainly in the ~800–1400 km offset range); 3) the coda wave trains decrease in length from ~8 s at ~800 km offset to 3–4 s at ~1400 km offset; 4) the scattered arrivals show very little lateral correlation. The four key observations are made in reversed sections along the different PNE profiles. These consistent observations show that the delayed and scattered arrivals must be caused by a depth dependent structure and not by lateral variations in the velocity structure along the PNE profiles. They cannot be caused by inhomogeneous near-surface low-velocity anomalies, i.e. sedimentary basins, because such structures would cause static-like features in the wavefield, which would be identifiable at certain positions along the seismic profile, and not always at approximately the same distance from the seismic sources.

We have modelled the scattered and delayed arrivals observed along PNE profile Kraton by a heterogeneous low-velocity zone from 100 to 180 km depth (cf. Thybo and Perchuc, 1997; Nielsen et al., 2002, 2003a; Thybo, 2006). Tomographic studies conducted along this line have shown the existence of a zone at ~100–180 km depth with a slightly reduced velocity as compared to the velocity structures above and below (Fig. 6; Nielsen et al., 1999). Note, however, that the average uppermost mantle velocities below profile Kraton are high (Fig. 6), and that the velocities in the ~50–200 km depth range are all higher than in the global IASP91 model (Kennett and Engdahl, 1991). We have tested many (>100) heterogeneous models (cf. Fig. 7) for representation of the scattering medium below ~100 km depth (e.g. Nielsen et al., 2002). The best fit to the observations is for a heterogeneous low-velocity zone with fluctuations described by a von Karman distribution function with a Hurst number of 0.5, a standard deviation of 2% of the background values of the elastic parameters, and horizontal and vertical correlation lengths of 5 and 3 km, respectively (Fig. 7a). This model explains the key observations of the scattering: the scattered arrivals are mainly restricted to offsets larger than 500–800 km; the duration of the scattered wave trains decrease from ~8 s at ~800 km offset to ~4 s at ~1400 km offset; only very little correlation of the scattered arrivals is evident. Vertically elongated anomalies provide a significantly

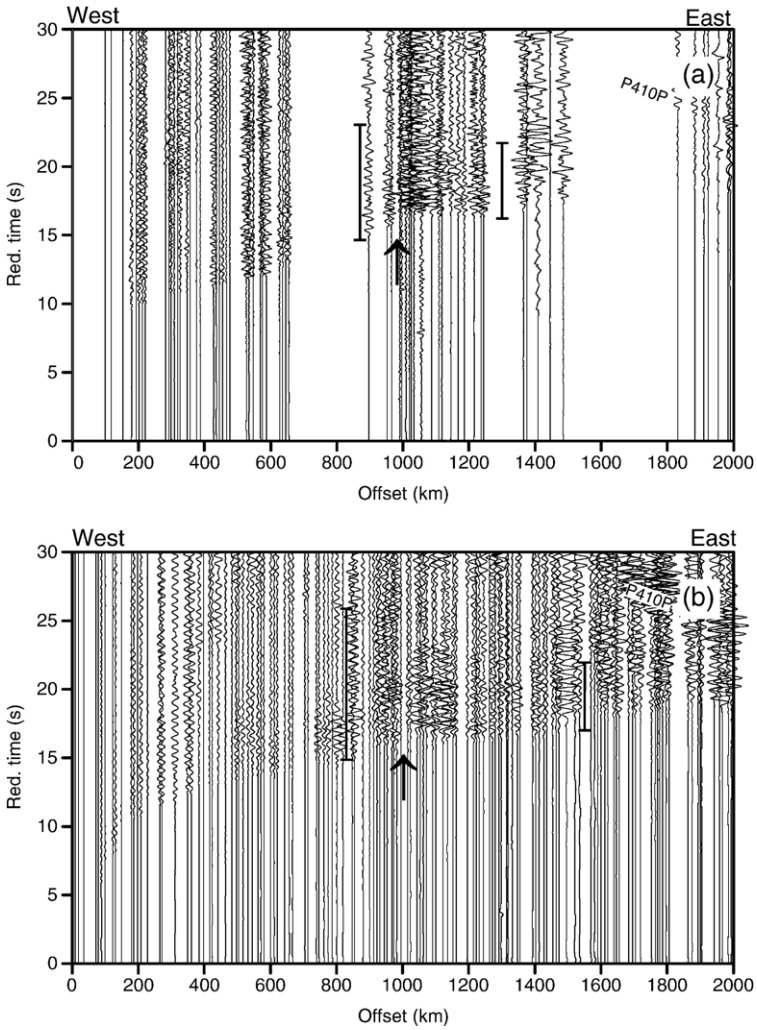

Fig. 5. PNE seismic sections of profile Kraton (cf. Fig. 1) plotted in reduced travel time format (reduction velocity of 8.7 km/s): (a) PNE 1, (b) PNE 2, (c) PNE 3, and (d) PNE 4. Vertical arrows indicate the travel time delays associated with the upper mantle low-velocity zone. Vertical bars indicate the approximate length of the scattered arrivals (coda) behind the first arrivals. P410P: Reflection from the top of the mantle transition zone. Amplitudes are scaled proportional to offset.

poorer fit to the observed scattering (Fig. 7b). The amplitudes in the ~800–1200 km offset range are too small for fluctuations with horizontal and vertical correlation lengths of 5 and 7 km, respectively. Fluctuations with relatively large horizontal correlation lengths also cannot explain the observed data (Fig. 7c). The model with horizontal and vertical correlations lengths of 30 and 3 km, respectively, causes scattered arrivals with a high degree of spatial correlation, inconsistent with the observations. Very fine-scale heterogeneity with correlation lengths below 1 km results in too weak scattering and too small amplitudes of the ~2 Hz scattered wave trains at offsets larger than ~800 km (Fig. 7d). The results (Fig. 7) are calculated for purely elastic models and inelastic damping in the crust and mantle layers has not been taken into account.

Heterogeneity in the crust and in the uppermost mantle from ~40 to 100 km depth cannot explain the scattered arrivals between ~800 and 1400 km offset (cf. Nielsen et al., 2003a). The lower crustal heterogeneity, which can account for the coda of the teleseismic Pn arrivals, is fine-grained and only causes insignificant scattering at frequencies of the ~2 Hz (Fig. 8a). Furthermore, the scattering observed from the lower crust is not restricted to the 800–1400 km offset interval. The uppermost mantle heterogeneity model suggested by Ryberg et al. (2000) also cannot account for the scattering characteristics that we observe from ~800 to ~1400 km offset (Fig. 8b). The mantle heterogeneity

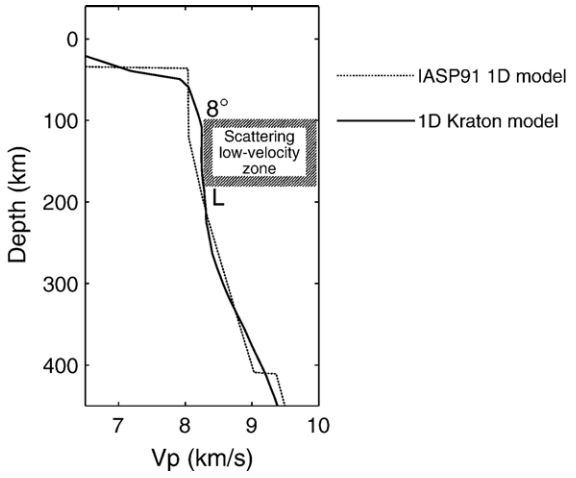

Fig. 6. 1D P-wave velocity profiles of the global IASP91 model (cf. Kennett and Engdahl, 1991) and the average of the tomographic first arrival travel time inversion model of PNE profile Kraton (cf. Nielsen et al., 1999). 8° and L mark the top and bottom of the low-velocity scattering zone.

from 40 to 100 km depth causes a ~3 s long coda to the mantle first arrivals at offsets larger than 200 km. This coda is not mainly restricted to the ~800–1400 km offset interval, and its duration is too short around 800–1100 km offset. We therefore conclude that a heterogeneous zone below 100 km depth is required in order to explain the scattering characteristics of the available PNE seismic profiles. The calculated response for the preferred model with 2% heterogeneity in the 100–180 km depth range (Fig. 8c) is calculated for a visco-elastic model including inelastic damping given by Qp and Qs values of 1000 and 600 in the mantle layers, Qp=500 and Qs=300 in the lower crust from 20 to 40 km depth, and Qp=200 and Qs=125 from 5 to 20 km depth. Strong attenuation (Qp- and Qs-values of 100 and 60) in the topmost part of the crust (0–5 km depth) accounts for damping effects of sedimentary structures and surface topography. The visco-elastic synthetic seismograms have a more correct amplitude decay with offset than the purely elastic results. Nielsen et al. (2003b) give a more thorough description of visco-elastic modelling of scattering effects in the upper mantle.

5. Heterogeneity around the top of the mantle transition zone

Strong reflections from the top of the mantle transition zone at about 410 km depth (P410) are observed in all available controlled-source seismic sections from the Russian cratonic regions and North America that extend to sufficient offset (Fig. 1). Furthermore, a reflection from a shallower depth (P320) is evident in the sections. Kinematic modelling of the P320 and P410 reflections indicate reflector depths of 310–350 and 400–430 km, respectively. Both the P320 and the P410 reflections are trailed by coda wavetrains with large amplitude, indicating the existence of a 100–140 km thick heterogeneous interval around the top of the mantle transition zone (Fig. 9; Thybo et al., 1997, 2003a).

The P320 reflection is most clearly identified in the ~1700–2400 km offset range, but it is observed from ~1400 to 1500 km offset (Fig. 9). The phase arrives about 4 s after the onset of the first arrival at ~1700 km offset, whereas it occurs only ~1–2 s later than the first arrival at 2200 km offset. The exact onset of the P320 reflectivity is most clearly observed at offsets smaller than 2000 km. For offsets larger than 2000 km the onset of the P320 typically interferes with scattered wavetrains behind the first arrivals and the P410. An up to ~5 s long coda of scattered arrivals is observed behind the P320 over the entire offset range where the phase is observed.

The P410 reflection is observed as a separate phase from ~1400 to ~2500 km offset. At ~1400–1500 km offset the onset of the P410 is observed ~10 s later than the first arrival and ~6–8 s behind the P320 reflection (Fig. 9). The P410 reflection is, in general, the strongest seismic arrival observed in the ~1600–2000 km offset range of the available data sections followed by an up to ~5 s long, strong coda of scattered arrivals. Beyond ~2000–2200 km offset, the P410 interferes with the coda wavetrains of the P320 arrival. The P320 and P410 reflections merge at ~2400–2500 km offset where the refracted arrival from the top of the transition zone constitutes the first arrival. This refracted wave arrives only 1–2 s before the merged P320 and P410 reflections of strong amplitude.

The above key observations regarding the kinematics and the coda characteristics of the P320 and P410 reflections are identified in the available high-resolution controlled-source record sections with data beyond 2000 km offset. The basic observations are consistently made in the same offset intervals on reversed sections, although small differences regarding the coda wave amplitudes may be observed in the different directions (see also Thybo et al., 2003a).

The P320 and P410 reflections show a characteristic amplitude variation with offset. The amplitudes of the P320 and P410 reflections increase abruptly around 1700–2000 km offset and 1600–1900 km offset, respectively. These amplitude variations indicate positive velocity contrasts at both the '320' and '410'

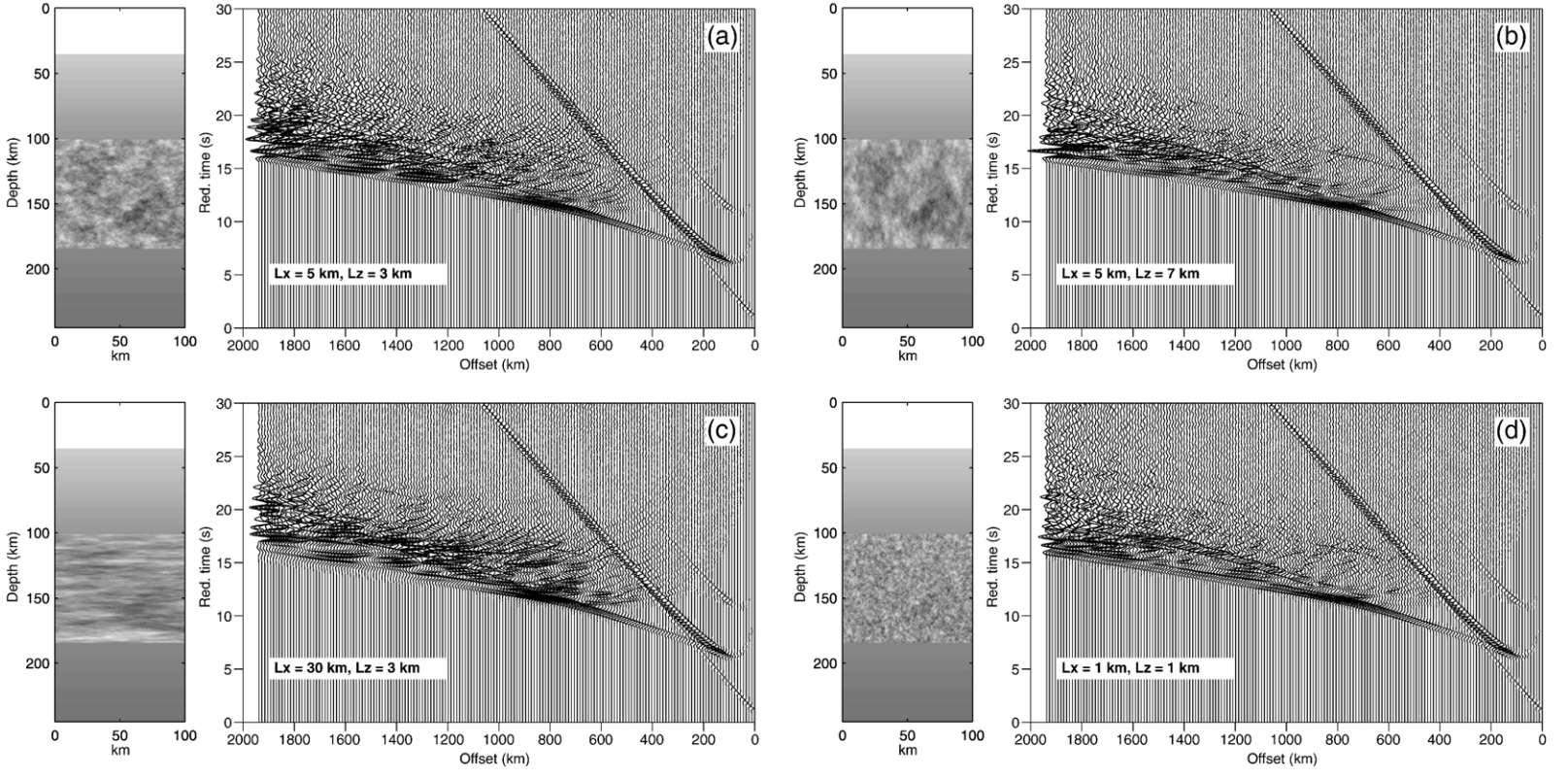

Fig. 7. Stochastic P-wave velocity models and their corresponding calculated seismic sections. Sphericity of the earth is accounted for by applying the corrections of Müller (1985) to the velocity models. The velocity fluctuations between 100 and 185 km depth follow a von Karman distribution with a Hurst number equal to 0.5 (exponential medium). They have a standard deviation equal to 2% of the average background velocity value. Lx and Lz are horizontal and vertical correlation lengths, respectively. Only 100 km of the 2000 km long models are shown. The amplitude scaling and the reduced travel time format of the seismic sections are the same as in Fig. 5.

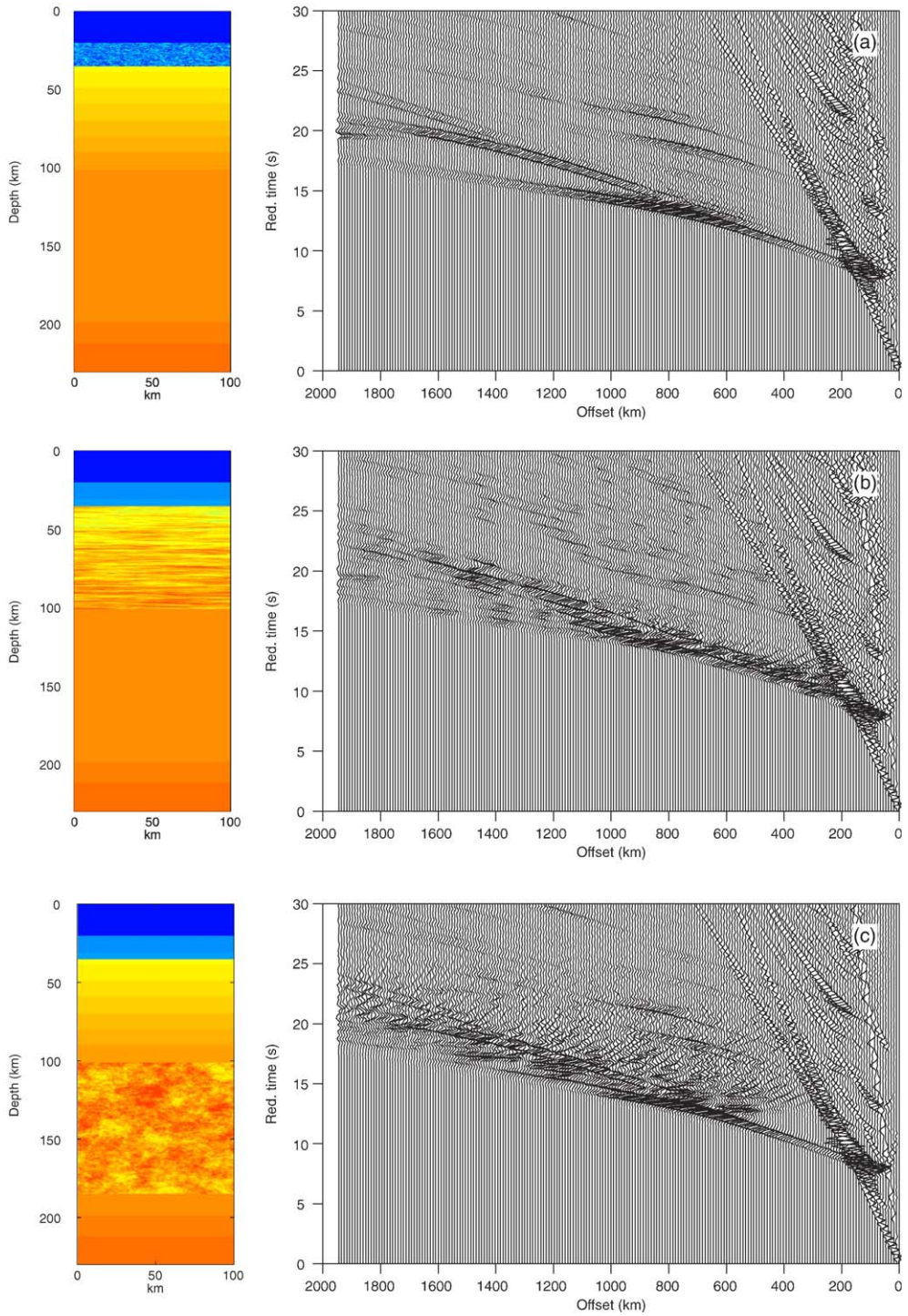

Fig. 8. Models with heterogeneous material in different depth intervals and the corresponding calculated seismic sections: (a) lower crustal scattering, (b) scattering in the uppermost mantle from the Moho to 100 km depth, and (c) scattering in the 100–185 km depth interval. Sphericity of the earth is accounted for by applying the corrections of Müller (1985) to the velocity models. The calculated data sections are shown in the same reduced travel time format and with the same amplitude scaling as the observed data of Fig. 5.

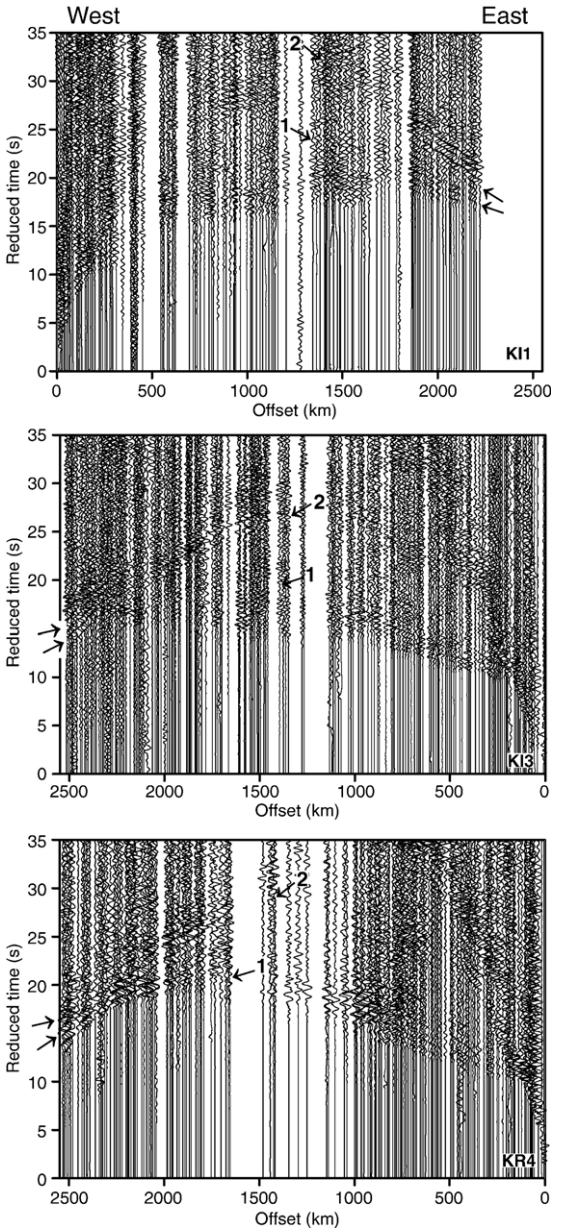

Fig. 9. Trace-normalized seismic sections plotted in reduced travel time versus offset from the seismic source (reduction velocity of 8.7 km/s). KI1, KI3, and KR4 refer to PNE sections Kimberlite 1, 2 and Kraton 4. The onset of the seismic reflectivity from around the top of the Transition Zone (P320) is indicated by the tilted arrows marked by "1", and the reflection from the '410' reflector is indicated by arrows marked by "2".

reflecting interfaces. Reflectivity calculations in one-dimensional models (cf. Fuchs and Müller, 1971; Müller, 1985) and in two-dimensional models of the P320 and P410 reflections observed in the Russian PNE sections indicates that the '320' and '410' reflectors are gradient zones (Thybo et al., 2003a). The absence of strong reflected P320 signals at offsets shorter than 1700 km offset is explained by a gradual velocity change at 320 km depth where the '320' reflector is a 20 km wide gradient zone with a total velocity increase of 0.24 km/s. The '410' is modelled as a 30 km thick gradient zone with a total increase in velocity of 0.47 km/s.

The pronounced coda wavetrains of the P320 and P410 reflections do not show any lateral correlation. This indicates small scattering bodies compared to the Fresnel zone radius, which is on the order of 50–150 km for the dominant P-waves. From visco-elastic full waveform seismic calculations, we find that a model with a 140 km thick heterogeneous zone around the top of the mantle transition zone (Fig. 10) explains the main characteristics of the codas of the P320 and P410 reflections, whereas a model without heterogeneity in this depth range cannot explain observations (cf. Thybo et al., 2003a). The calculated seismic section is similar to the observations regarding the duration of the high-amplitude coda of the P320 and P410 reflections in the 1400–2400 km offset range but it does not reproduce the ~5 s long coda of scattered arrivals observed where the P320 and P410 reflections interfere directly behind the first arrival at 2400–2500 km offset (compare Figs. 9 and 10). The heterogeneity is described by a von Karman correlation function with a Hurst number of 0.5, a standard deviation of 2% of the background model parameter values, and horizontal and vertical correlation lengths of 20 and 5 km, respectively (Thybo et al., 2003a). Tests have shown that correlation lengths in the range of 10–40 km (horizontally) and 2–10 km (vertically) explain the observed scattering features at the resolution of the seismic signals from the top of the transition zone.

6. Discussion

6.1. Lower crustal heterogeneity

Lower crustal heterogeneity causes a coda of scattered arrivals to upper mantle arrivals. In particular, the teleseismic (or long-range) Pn phase, which propagates as multiply reflected refractions along the underside of the Moho to large distances, is strongly influenced by lower crustal scattering with frequency dependent coda characteristics. For low frequencies (0–2.5 Hz), the amplitude of the coda is weak relative to the onset amplitudes of the teleseismic Pn, whereas the coda is relatively stronger in the mid-frequency (2.5–5 Hz) and in the high-frequency (5–10 Hz) ranges (Fig. 2). This frequency dependence of the coda characteristics is

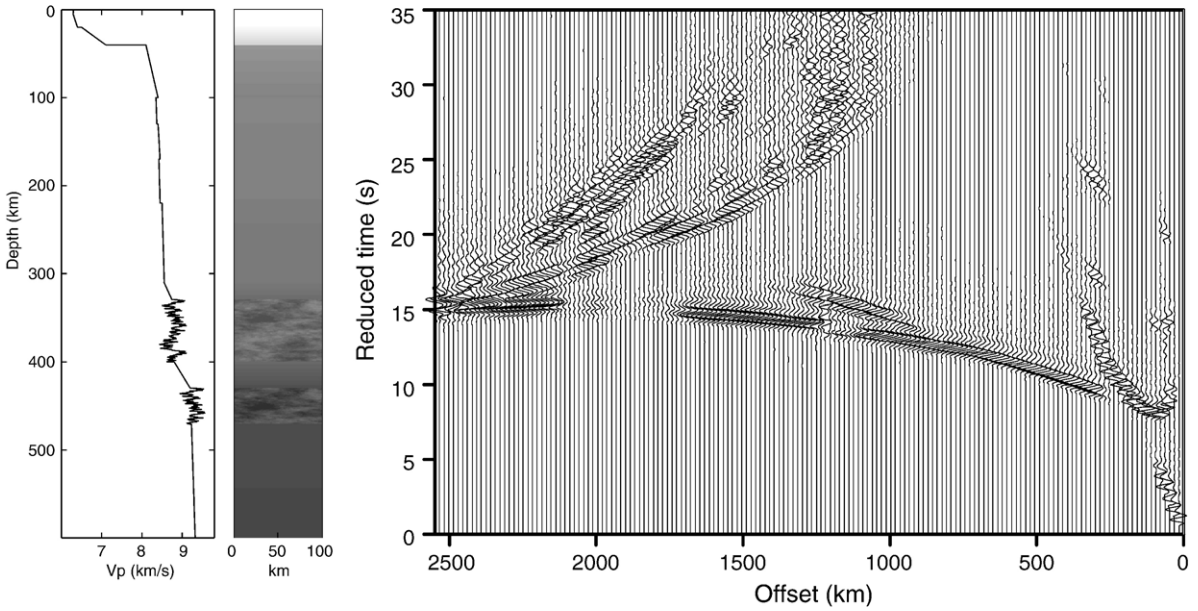

Fig. 10. Seismic velocity model including heterogeneity around the top of the mantle transition zone (left) and the corresponding 2-D visco-elastic finite-difference waveform response (right). Only a 100 km wide portion of the 2500 km long model is shown. The 1D velocity profile is extracted from this portion of the model. Sphericity of the earth is accounted for by applying the corrections of Müller (1985) to the velocity model. The source used for the synthetic seismic section is a Ricker wavelet with a central frequency of 2 Hz.

determined by the size of the fluctuations that cause the scattering. Fine-scale heterogeneity will cause scattering of high-frequency signals with only limited effect on low-frequency signals, whereas coarse-grained heterogeneity will cause scattering of the low-frequency signals. Nielsen and Thybo (2003) show that lower crustal fluctuations of the elastic parameters simulated by a von Karman distribution function with a Hurst number of 0.3 explain the teleseismic Pn coda observations for horizontal correlation lengths between 0.8 and 2.4 km and vertical correlation lengths between 0.2 and 0.6 km. Holliger and Levander (1992) analysed maps of exposed lower crustal rocks in the Ivrea zone of northern Italy. They showed that the lower crustal heterogeneity can be described by a von Karman distribution function with a Hurst number of 0.3 and horizontal and vertical correlation lengths of ~0.8 and ~0.2 km, respectively.

Numerous high-resolution normal-incidence seismic data sections collected in different continental areas typically show a reflective lower crust and a more transparent uppermost mantle down to ~20 s travel time, consistent with our preferred model for explaining the teleseismic Pn coda (Fig. 11; McGeary and Warner,

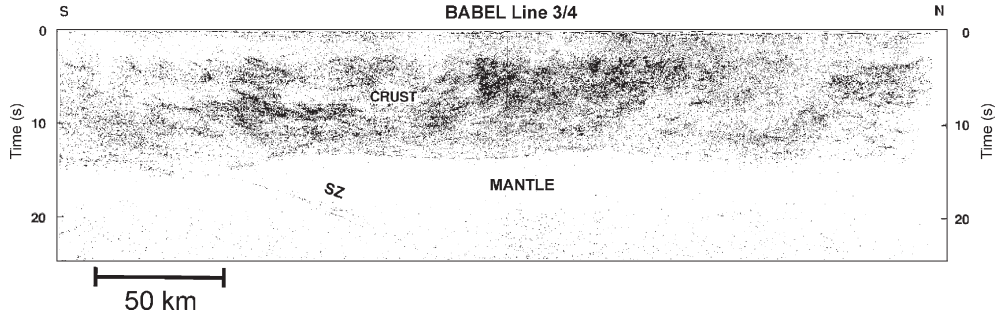

Fig. 11. Normal-incidence reflection seismic section collected in the Gulf of Bothnia during the BABEL experiment (cf. Fig. 1; BABEL Working Group, 1993). Note the numerous crustal reflections and the sparse reflectivity of the uppermost mantle. The isolated upper mantle dipping event (SZ) may represent a remnant subducted oceanic crust (BABEL Working Group, 1993; Balling, 2000).

1985; Bois and ECORS Working Group, 1991; BABEL Working Group, 1993; MONA LISA Working Group, 1997). Our results are consistent with a general model of continental areas with a heterogeneous lower crust and a more transparent uppermost mantle.

We reject a previously published model, which explains the teleseismic Pn coda by upper mantle scattering (Ryberg et al., 2000). The rejected model fits the high-frequency characteristics of the teleseismic Pn coda, but it is in conflict with the observations regarding the low-frequency coda and the relative kinematics of the teleseismic Pn and the first-arrival P-wave.

We have limited ourselves to studying lower crustal heterogeneity effects on the teleseismic Pn coda. Upper crustal structures such as surface topography, thick sedimentary basins and large fault systems may contribute further to the coda of the telseismic Pn (e.g. Morozov et al., 1998; Morozov and Smithson, 2000; Revenaugh, 1995).

6.2. Heterogeneity in the 100–200 km depth range

Densely sampled data with a high-frequency content (2–4 Hz) and reverse coverage of the delayed and scattered arrivals in the ~800–1400 km offset range are required for detection and modelling of the heterogeneous low-velocity zone below ~100 km depth. All available PNE seismic sections from the former Soviet Union indicate the existence of such a 50–100 km thick heterogeneous low-velocity zone, and we conclude that it is most likely a general phenomenon of cratonic regions. Global network earthquake data does not provide dense sampling of the ~800–1400 km offset range, and is typically dominated by low-frequency signals (<1 Hz). Therefore, such data is not suited for imaging the heterogeneous low-velocity zone below 100 km depth. The global tomographic images are typically deviations from a standard earth model, e.g. PREM (Dziewonski and Anderson, 1981) or IASP91 (Kennett and Engdahl, 1991). In the cratonic areas of Russia, all PNE data that we have investigated show upper mantle velocities from ~40–200 km depth which are all above the standard earth model values. Therefore, the global tomographic models show positive anomalies throughout the Siberian upper mantle, independent of the existence of a possible low-velocity zone in the high-velocity mantle.

Abramovitz et al. (2002) identified the low-velocity scattering zone below ~90–100 km depth in the Baltic Shield area from tomographic travel time inversion of P- and S-wave arrivals picked in the Fennolora data sections to about 2000 km distance from the seismic sources. The S-waves observed in the Fennolora data sections are strongly attenuated at ~800–1100 km offset, indicating a very small Qs-value in the low-velocity zone. The travel time modelling also indicates a high Poisson's ratio in the low-velocity zone. Thybo and Perchuc (1997) suggest that the heterogeneous low-velocity zone below ~100 km depth (the 8° discontinuity) is a global feature, and they explain the low velocity and heterogeneity of the zone by slight partial melting of the mantle rocks. Temperatures close to the solidus or the presence of, even small amounts of, molten material may explain the velocity reduction and scattering features of the ~100–200 km depth range (cf. Thybo and Perchuc, 1997; Sato et al., 1989; Nielsen et al., 2002). In the model of Thybo and Perchuc (1997), melts from the ~100–200 km depth range will not rise to the surface. They will solidify just above 100 km depth due to a characteristic kink in the solidus curve for mantle rocks that contain water and carbon dioxide (cf. Wyllie, 1980). The hypothesis of high temperatures and the possible presence of partial melt is consistent with the high Poisson's ratios and small Qs-values observed for the low-velocity zone in the Baltic Shield. Morozova et al. (2000) identify a low-Q zone below ~100 km depth in the East European Craton, consistent with the findings from the Baltic Shield. It is not known if the small Q-values should mainly be explained in terms of scattering effects or by intrinsic absorption of the seismic energy. Inelastic damping resulting from e.g. small amounts of partial melt could reduce the amplitude of the scattered arrivals from the mantle low-velocity zone. If the low-velocity zone is in a state of partial melting or close to the point of melting, S-wave velocities would expectedly be abnormally low and Poisson's ratio high, consistent with the observations from the Baltic Shield. High Poisson's ratio could lead to stronger scattering.

Sub-horizontal reflectivity is often observed at 20–25 s travel time (~80–100 km depth) in high-resolution normal-incidence seismic sections collected in different parts of the world (e.g. MONA LISA Working Group, 1997; Steer et al., 1998; Fig. 12). These reflections may mark the top of the heterogeneous mantle low-velocity zone or sill-like structures created by melts from the low-velocity zone that have risen to solidify slightly above the low-velocity zone (cf. Thybo, 2006).

6.3. Heterogeneity at the top of the transition zone

Our modelling of the P320 and the P410 reflections from around the top of the mantle transition zone and their coda characteristics is mainly

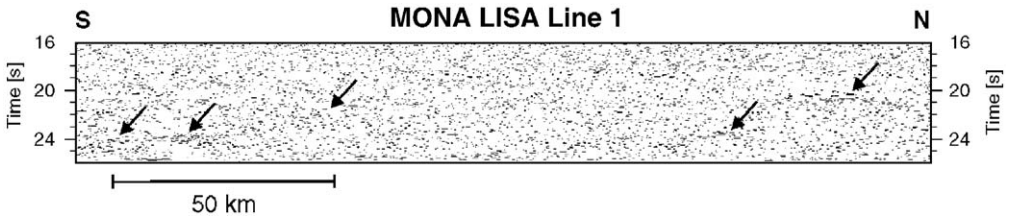

Fig. 12. Normal-incidence reflection seismic section collected in the southeastern North Sea during the MONA LISA experiment (cf. Fig. 1; MONA LISA Working Group, 1997). Tilted arrows indicate sub-horizontal reflections at 20–25 s travel time (~80–100 km depth).

based on observations made in the Russian PNE data sets. Lewis and Meyer (1968) interpreted the far-offset recordings of seismic waves from large chemical explosions (30 tonnes of explosives) detonated in Lake Superior during the Early Rise experiment (cf. Fig. 1). They interpreted the existence of two reflectors at around 350 km depth and 450 km depth along the west-striking seismic transect (profile 6) (Fig. 13). These findings are generally consistent with our interpretations from the Russian cratonic regions except for slight differences in the depths to the reflectors. Lewis and Meyer (1968) model the reflector at ~350 km depth as a ~20 km thick transition zone with a ~0.25 km/s velocity increases, consistent with our findings for the '320' reflector. Further they find that the remarkably deep '410' reflector at ~450 km depth is a first order discontinuity with a velocity increase of 0.6 km/s. We find that, in the Russian cratonic regions, the '410' reflector is a ~30 km wide gradient zone where the velocity on average increases by ~0.47 km/s. The Early Rise data section also shows pronounced codas

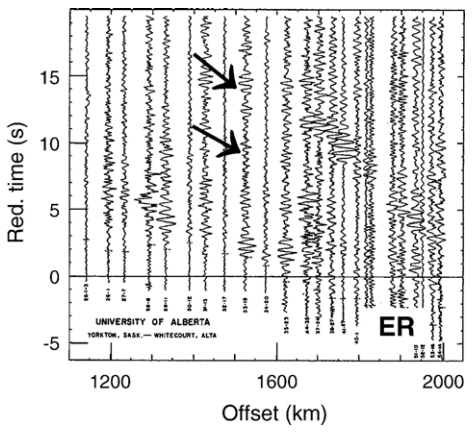

Fig. 13. Close-up of a seismic record section from the early Rise experiment in North America (cf. Fig. 1; Lewis and Meyer, 1968). The section is plotted in reduced travel time format (reduction velocity of 8.0 km/s). Tilted arrows indicate the P320 and P410 reflections.

of up to ~5 s duration trailing the two reflections from around the top of the transition zone, consistent with the observations in the Russian PNE sections.

Song et al. (2004) found a low-velocity zone atop the '410' discontinuity in the western parts of the USA based on analysis of earthquake-generated refracted waves and receiver functions. They discuss that this low-velocities zone may indicate an unusual high water content around the '410' and that it might be linked to tectonic processes related to subduction of the Farallon plate and surface extension in the back-arc regime. Song et al. (2004) note that reported low-velocity zones above the '410' discontinuity are normally associated with back-arc regimes of ongoing subduction or ancient subduction. Fee and Dueker (2004) identified a low-velocity zone above the '410' discontinuity in the area of the Yellowstone hotspot using common conversion point imaging of P-wave receiver functions. Revenaugh and Sipkin (1994) interpreted a seismic boundary at ~330 km depth based on analysis of multiply reflected low-frequency ScS phases from the Earth's core–mantle boundary. The results of Revenaugh and Sipkin (1994) show a negative reflection coefficient at 330 km depth and, thus, indicate a negative velocity contrast at this depth. We have interpreted positive velocity contrasts at both the '320' and '410' reflectors. This apparent conflict between our results and the findings based on the earthquake data may be caused by the different frequency contents of the PNE data and the recordings of earthquakes (cf. Thybo et al., 2003a). The frequency content is about an order of magnitude higher for the PNE data than for the earthquake recordings. For the short wavelengths of the PNE data, the top of the scattering zone at ~320 km depth may correspond to a positive velocity contrast caused by the heterogeneity in the interval. The long-wavelength earthquake-generated waves sample a relatively thick part of the scattering depth interval, which potentially may correspond to a velocity reversal compared to the layers above.

The reflectivity observed in the Russian and North American cratonic regions indicates that the existence of the '320' and '410' reflectors as well as significant

heterogeneity around the top of the transition zone may possibly be a general feature of continental regions. The onsets of the P320 and P410 reflections are typically less than 5 s apart for offsets larger than 2000 km. High-frequency data with dense spatial sampling are required in order to unequivocally separate the two phases. Erroneous interpretation of the P320 as the P410 reflection will lead to severe misinterpretation of the depth to the mantle transition zone.

Thybo et al. (2003a) favour to explain the pronounced heterogeneity by α-β-γ spinel transformations. The ~140 km thick interval over which the transformations take place (from ~320 to ~460 km depth) is explained by a highly variable high iron content of up to 17% in the relevant depth range. Stacked, subducted slabs as well as transformations of pyroxenes into garnet may also contribute to the observed scattering of the seismic signals. Thybo et al. (2003a) conclude that the presence of water or partial melts are unlikely candidates for explaining the scattering around the top of the transition zone.

6.4. Composite model response

We have calculated the two-dimensional visco-elastic full waveform seismic section for a model which includes all three strongly heterogeneous zones: the lower crust; the 100–180 km depth interval, and the 140 km thick zone around the top of the mantle transition zone (Fig. 14). The source used for the synthetic calculation has a centre frequency of 2 Hz as in the calculations regarding the heterogeneous 100–200 km and 320–460 km depth intervals. Therefore, the synthetic wavefield is only weakly influenced by the fine-scale lower crustal heterogeneity, and the extensive high-frequency coda of the teleseismic Pn is not present in the section. The synthetic data section provides a good match to all the main scattering features observed in the ~800–2500 km offset interval of the Russian PNE data (compare Fig. 14 to the observed sections of Fig. 9). The composite model section matches the up to ~8 s long coda wavetrains associated with the heterogeneous zone at 100–180 km depth, the irregular, scattered and damped first arrivals for offsets larger than 1000 km, and the long high-amplitude scattered wavetrains behind the P320 and P410 reflections. Note that the composite model also reproduces the ~5 s long coda behind the interfering P320 and P410 reflections in the 2400–2500 km offset range, which could not be explained by the heterogeneous medium at the top of the transition zone alone. The composite model also results

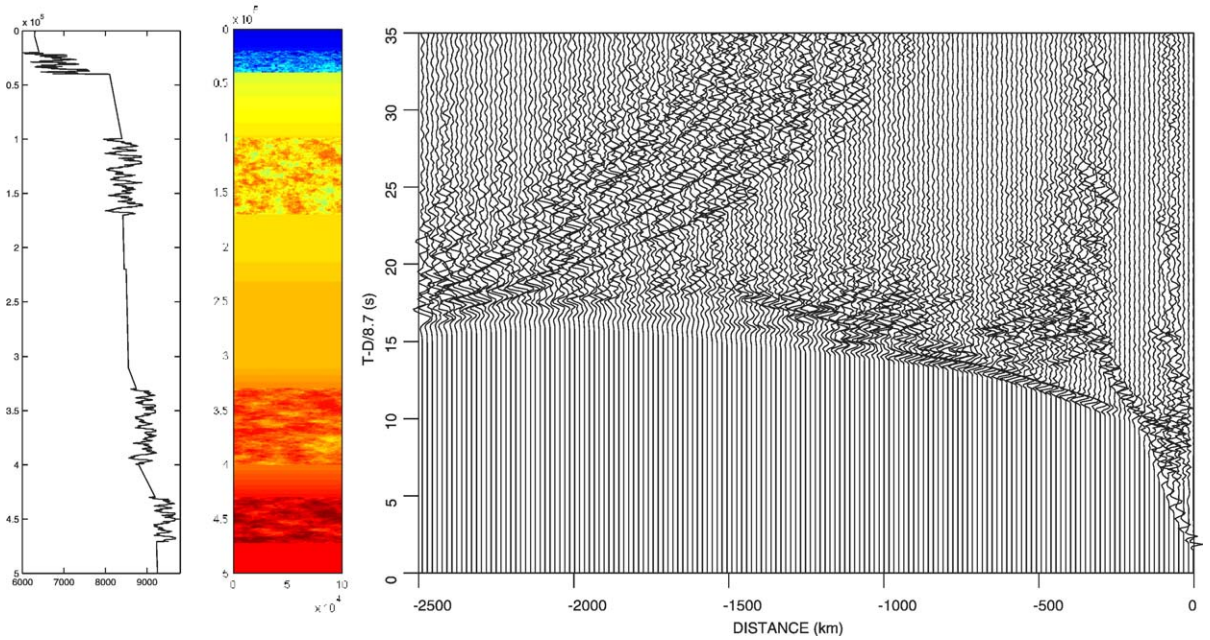

Fig. 14. Left: Seismic velocity model including heterogeneity at three depth levels: 1) the lower crust from 20 to 40 km depth, 2) the 100–185 km depth interval, and 3) around the top of the mantle transition at 320–460 km depth. Only a 100 km wide portion of the 2500 km long model is shown. The 1D velocity profile is extracted from this portion of the model. Sphericity of the earth is accounted for by applying the corrections of Müller (1985) to the velocity model. Right: The 2-D visco-elastic finite-difference waveform response calculated for the model shown to the left. The source used for the synthetic seismic section is a Ricker wavelet with a central frequency of 2 Hz.

in a more even and widespread distribution of the scattered signals, consistent with observations. It is evident that scattering in the shallower heterogeneous zones of the model contributes substantially to the complexity of signals from deeper levels.

6.5. Two-dimensional modelling of three-dimensional structures

The heterogeneous layers of the crust and upper mantle are expected to have a three-dimensional structure of the inherent heterogeneity. Computational limitations restrict us to two-dimensional wavefield calculations. Calculation of the full wavefield in large-scale three-dimensional, heterogeneous models of the deep crust and upper mantle by finite-difference techniques is not practically feasible on present-day computers available to the scientific community. Our previous modelling results show that two-dimensional media tend to generate longer scattering codas than one-dimensional media (Nielsen et al., 2001, 2002). However, we cannot quantify the parts of the spatial propagation and scattering effects in the three-dimensional Earth structures that are not accounted for by the two-dimensional modelling.

7. Conclusions

Three heterogeneous zones have been identified in the crust and upper mantle based on interpretation and modelling of Russian PNE data: 1) the lower crust from ~20 to ~40 km depth; 2) the 100–180 km depth interval; and 3) a ~140 km thick interval around the top of the mantle transition zone.

The positive vertical velocity gradient in the uppermost mantle beneath the Siberian cratonic region and the heterogeneous lower crust from ~20 to ~40 km depth cause generation of whispering-gallery arrivals with extensive codas and apparent upper mantle velocities of 8.1–8.4 km/s which are observed to offsets of more than 3000 km. These arrivals correspond to the so-called teleseismic Pn phases which have been prominently observed over a broad range of frequencies (0–10 Hz) along PNE profiles Quartz and Ruby in the Russian cratonic regions.

The heterogeneous zone below 100 km depth causes scattering of the seismic wavefield at the main frequencies (2–4 Hz) of the PNE data. These scattered arrivals are observed as a coda to the first arrivals in the ~800–1400 km offset range. By two-dimensional modelling we explain these observations along profile Kraton in Siberia by heterogeneity in the 80 km thick upper mantle low-velocity zone below 100 km depth. This heterogeneous medium is represented by fluctuations described by a von Karman distribution function with a Hurst number of 0.5 and spatial correlation lengths of 5–10 km (horizontally) and 3–5 km (vertically). Reflections observed at ~20–25 s travel time in normal-incidence seismic record sections in other regions may represent reflectors around the top of this heterogeneous low-velocity zone, which may be a global feature.

Heterogeneous media around the top of the mantle transition zone cause ~5 s long wavetrains of scattered arrivals behind the reflections from 320 and 410 km depth observed in the Russian PNE seismic sections. Similar observations are made in controlled-source seismic sections from North America. Inclusion of fluctuations in the 320–460 km depth interval with horizontal and vertical correlation lengths on the order of 20–40 and 5–10 km, respectively, leads to synthetic seismograms that match the observed scattered signals.

The different heterogeneous zones can be uniquely interpreted from the seismic data sections, because the scattered arrivals from the zones are consistently identified in different, well-defined offsets intervals in reversed seismic sections.

Acknowledgments

This study was financed by the Carlsberg Foundation and the Danish Natural Science Research Council. The waveform calculations were made on the computer facilities of the Danish Center for Scientific Computing (DCSC). Johan Robertsson provided the visco-elastic finite-difference codes used for the seismic modelling. The reviews of Robert W. Clayton and an anonymous reviewer are acknowledged.

References

Abramovitz, T., Thybo, H., Perchuc, E., 2002. Tomographic inversion of seismic P- and S-wave velocities from the Baltic Shield based on FENNOLORA data. Tectonophysics 358, 151–174.

BABEL Working Group, 1993. Deep seismic reflection/refraction interpretation of crustal structure along BABEL profiles A and B in the southern Baltic Sea. Geophysical Journal International 112, 325–343.

Balling, N., 2000. Deep seismic reflection evidence for ancient subduction and collision zones within the continental lithosphere of northwestern Europe. Tectonophysics 329, 269–300.

Bijwaard, H., Spakman, W., 2000. Non-linear global P-wave tomography by iterated linearized inversion. Geophysical Journal International 141, 71–82.

Bois, C., ECORS Working Group, 1991. Late- and post-orogenic evolution of the crust studied from ECORS deep seismic profiles. In: Meissner, R., Brown, L., Dürbaum, H.-J., Franke, W., Fuchs, K., Seifert, F. (Eds.), Continental Lithosphere: Deep Seismic Reflections. AGU Geodynamics Series, 1991, pp. 59–68.

Dziewonski, A.M., Anderson, D.L., 1981. Preliminary reference Earth model. Physics of the Earth and Planetary Interiors 25, 297–356.

Ekström, G., Dziewonski, A.M., 1998. The unique anisotropy of the Pacific upper mantle. Nature 394, 168–172.

Fee, D., Dueker, K., 2004. Mantle transition zone topography and structure beneath the Yellowstone hotspot. Geophysical Research Letters 31. doi:10.1029/2004GL020636.

Fuchs, K., Müller, G., 1971. Computation of synthetic seismograms with the reflectivity method and comparison with observations. Geophysical Journal of the Royal Astronomical Society 23, 417–433.

Fukao, Y., Sri, W., Obayashi, M., 2001. Stagnant slabs in the upper and lower mantle transition region. Reviews of Geophysics 39, 291–323.

Holliger, K., Levander, A.R., 1992. A stochastic view of lower crustal fabric based on evidence from the Ivrea zone. Geophysical Research Letters 19, 1153–1156.

Kennett, B.L.N., Engdahl, E.R., 1991. Traveltimes for global earthquake location and phase identification. Geophysical Journal International 105, 429–465.

Lewis, B.T., Meyer, R.P., 1968. A seismic investigation of the upper mantle to the west of Lake Superior. Bulletin of the Seismological Society of America 58, 565–596.

McGeary, S., Warner, M.R., 1985. Seismic profiling the continental lithosphere. Nature 317, 795–797.

MONA LISA Working Group, 1997. Deep seismic investigations of the lithosphere in the south-eastern North Sea. Tectonophysics 269, 1–19.

Montelli, R., Nolet, G., Dahlen, F.A., Masters, G., Engdahl, E.R., Hung, S.-H., 2004. Finite-frequency tomography reveals a variety of plumes in the mantle. Science 303, 338–343.

Morozov, I.B., Smithson, S.B., 2000. Coda of long-range arrivals from nuclear explosions. Bulletin of the Seismological Society of America 90, 929–939.

Morozov, I.B., Morozova, E.A., Smithson, S.B., Solodilov, L.N., 1998. On the nature of the teleseismic Pn phase observed on the ultralong-range profile "Quartz," Russia. Bulletin of the Seismological Society of America 88, 62–73.

Morozova, E.A., Morozov, I.B., Smithson, S.B., 1999. Heterogeneity of the uppermost mantle beneath Russian Eurasia from the ultra-long-range profile QUARTZ. Journal of Geophysical Research 104, 20.329–20.348.

Morozova, E.A., Morozov, I.B., Smithson, S.B., Solodilov, L., 2000. Lithospheric boundaries and upper mantle heterogeneity beneath Russian Eurasia; evidence from the DSS profile QUARTZ. In: Carbonell, R., Gallart, J., Torne, M. (Eds.), Deep Seismic Profiling of the Continents and their Margins. Tectonophysics, vol. 329, pp. 333–344.

Müller, G., 1985. The reflectivity method: a tutorial. Journal of Geophysics 58, 153–174.

Nielsen, L., Thybo, H., 2003. The origin of teleseismic Pn waves: multiple crustal scattering of upper mantle whispering-gallery phases. Journal of Geophysical Research 108. doi:10.1029/2003JB002487.

Nielsen, L., Thybo, H., Solodilov, L., 1999. Seismic tomographic inversion of Russian PNE data along profile Kraton. Geophysical Research Letters 22, 3413–3416.

Nielsen, L., Thybo, H., Egorkin, A.V., 2001. Constraints on reflective bodies below the 8° discontinuity from reflectivity modelling. Geophysical Journal International 145, 759–770.

Nielsen, L., Thybo, H., Egorkin, A.V., 2002. Implications of seismic scattering below the 8° discontinuity along PNE profile Kraton. Tectonophysics 358, 135–150.

Nielsen, L., Thybo, H., Levander, A., Solodilov, L., 2003a. Origin of upper mantle seismic scattering—evidence from Russian PNE data. Geophysical Journal International 154, 196–204.

Nielsen, L., Thybo, H., Morozov, I.B., Smithson, S.B., Solodilov, L., 2003b. Teleseismic Pn arrivals: influence of upper mantle velocity gradient and crustal scattering. Geophysical Journal International 153, F1–F7.

Revenaugh, J., 1995. The contribution of topographic scattering to teleseismic coda in Southern California. Geophysical Research Letters 22, 543–546.

Revenaugh, J., Sipkin, S.A., 1994. Seismic evidence for silicate melt atop the 410-km mantle discontinuity. Nature 369, 474–476.

Robertsson, J.O.A., Blanch, J.O., Symes, W.W., 1994. Viscoelastic finite-difference modeling. Geophysics 59, 1444–1456.

Romanowicz, B., Gung, Y., 2002. Superplumes from the core–mantle boundary to the lithosphere; implications for heat flux. Science 296, 513–516.

Ross, A.R., Thybo, H., Solodilov, L.N., 2004. Reflection seismic profiles of the core–mantle boundary. Journal of Geophysical Research 109 (B08303). doi:10.1029/2003JB002515.

Ryberg, T., Fuchs, K., Egorkin, A.V., Solodilov, L., 1995. Observation of high-frequency teleseismic Pn waves on the long-range Quartz profile across northern Eurasia. Journal of Geophysical Research 100, 18.151–18.163.

Ryberg, T., Wenzel, F., Mechie, J., Egorkin, A.V., Fuchs, K., Solodilov, L., 1996. 2D velocity structure beneath northern Eurasia derived from super long-range seismic profile QUARTZ. Bulletin of the Seismological Society of America 86, 857–867.

Ryberg, T., Tittgemeyer, M., Wenzel, F., 2000. Finite difference modelling of P-wave scattering in the upper mantle. Geophysical Journal International 141, 787–800.

Sato, H., Sacks, I.S., Murase, T., 1989. The use of laboratory velocity data for estimating temperature and partial melt fraction in the low-velocity zone: comparison with heat flow and electrical conductivity studies. Journal of Geophysical Research 94, 5689–5704.

Selby, N.D., Woodhouse, J.H., 2002. The Q structure of the upper mantle; constraints from Rayleigh wave amplitudes. Journal of Geophysical Research 107. doi:10.1029/2001JB000257.

Song, T.-R.A., Helmberger, D.V., Grand, S.P., 2004. Low-velocity zone atop the 410-km seismic discontinuity in the northwestern United States. Nature 427, 530–533.

Steer, D., Knapp, J.H., Brown, L.D., Echtler, H.P., Brown, D.L., Berzin, R., 1998. Deep structure of the continental lithosphere in an unextended orogen; an explosive-source seismic reflection profile in the Urals (Urals Seismic Experiment and Integrated Studies (URSEIS 1995)). Tectonics 17, 143–157.

Thybo, H., 2006. The heterogeneous upper mantle low-velocity zone. Tectonophysics. 416, 53–79. doi:10.1016/j.tecto.2005.11.021 (this volume).

Thybo, H., Perchuc, E., 1997. The seismic 8° discontinuity and partial melting in continental mantle. Science 275, 1626–1629.

Thybo, H., Perchuc, E., Pavlenkova, N., 1997. Two reflectors in the 400 km depth range revealed from peaceful nuclear explosion seismic sections. In: Fuchs, K. (Ed.), Upper Mantle Heterogeneities

from Active and Passive Seismology. Kluwer Academic Publishers, Dordrecht, pp. 97–104.
Thybo, H., Nielsen, L., Perchuc, E., 2003a. Seismic scattering at the top of the mantle transition zone. Earth and Planetary Science Letters 216, 259–269.
Thybo, H., Ross, A.R., Egorkin, A.V., 2003b. Explosion seismic reflections from the earth's core. Earth and Planetary Science Letters 216, 693–702.
Tittgemeyer, M., Fuchs, K., Wenzel, F., 1996. Wave propagation in a multiple scattering upper mantle—observation and modelling. Geophysical Journal International 127, 492–502.
Tittgemeyer, M., Wenzel, F., Ryberg, T., Fuchs, K., 1999. Scales of heterogeneities in the continental crust and upper mantle. Pure and Applied Geophysics 156, 29–52.
Wyllie, P.J., 1980. The origin of kimberlite. Journal of Geophysical Research 85, 6902–6910.